Uranus' Magnetic Field and Particle Drifts in its Inner-Magnetosphere

Shan Gao, C. Wing Ho, and Tian-Sen Huang

Department of Physics, Prairie View A & M University

Prairie View, TX 77446

Telephone / Fax: (409) 857-2859 / (409) 857-4148

Claudia J. Alexander

Jet Propulsion Laboratory

Pasadena, CA 91109

Abstract. Both the Q_3 model (dipole and quadrupole) and OCT model (Q_3 plus octupole) of **Uranus' magnetic field** within 5 R_U are expressed in α and β (Euler Potentials) coordinate systems. By using the α and β coordinates of magnetic fields we calculate the drift paths and velocities for the zero second invariant ($J = 0$) charged particles with different total energies. Many aspects of Uranus' magnetic field are similar to those of Neptune [*Ho et al.*, 1997], such as a warped zero magnetic scalar potential surface and a region of local distorted magnetic field lines that gives rise to a large "open" area on the planetary surface when the field lines are mapped from this region. It is found that the OCT model gives a map of magnetic field coordinates on the planetary surface that explains the **Voyager 2**'s UVS data of *Herbert and Sandel* [1994] better than the Q_3 model. The grossly distorted α and β contours on the planetary surface may explain the incomplete **aurora circles** round both magnetic poles, and weak **UV emissions** are found lying along a belt that coincides remarkably well with the OCT magnetic equator. In addition, tracing of drift paths of $J = 0$ **charged particles** shows that the weak emission along the magnetic equator is due to the precipitation of $J = 0$ particles, or particles with a large equatorial pitch angle. Particularly, the low energy $J = 0$ particles tend to drift towards a planet in three concentrated regions where UV emissions are observed.

1. Introduction

Analyses of Voyager 2 (V2)'s magnetometer data [*Ness et al.*, 1986; *Connerney et al.*, 1987] show that the magnetic field of Uranus is complex and unique among all the known planetary magnetic fields (a similar complex field was later discovered during V2's visit to Neptune). For instance, the quadrupole components of the field are comparable in magnitude to the dipole. Also, a surprisingly large tilt (60^{o} to the rotation axis) and offset (0.33 R_U from the planetary center) of the magnetic dipole axis were found along with an almost sun-planet aligned rotation axis. The large tilted dipole has consequences such as large traversals of the Uranian moons over a wide range of magnetic latitudes and longitudes, resulting in peculiar particle absorption signatures [*Mauk et al.*, 1987; *Acuna et al.*, 1988]. The near sun-planet aligned rotation axis leads to the speculation of a convection dominated Uranian magnetosphere at the epoch during V2's visit [*Selesnick and Richardson*, 1986; *Vasyliunas*, 1987].

The first magnetic field model for Uranus is the Offset Tilted Dipole (OTD) model [*Ness et al.*, 1986]. Although the OTD model provides only a fair approximation to the field even beyond V2's closest approach of 4.2 R_U (1 R_U= 25,600 *km*), it is still useful for studying charged particle motions in the magnetosphere. A more accurate description for Uranus' magnetic field is the Q_3 model of *Connerney et al.* [1987] who utilized the generalized inverse techniques to obtain a spherical harmonic expansion of the internal field. Due to the relatively large closest approach distance of V2, only three terms (up to and including the octupole) of the expansion were obtained. The limited spatial distribution

of the available data restricts the reliability of the model to only the dipole and quadrupole while the octupole are largely unresolved. The use of only the first two terms out of an available three constitutes the Q_3 model. Nevertheless, the effect of using only the first two terms to calculate the predicted locations for absorption of energetic charged particles by the Uranian moons is significant, and the magnetic equator derived from the Q_3 model is warped and noticeably distorted from the plane surface associated with the OTD model [*Acuna et al* ., 1988]. The Q_3 model, however, cannot account for some significant discrepancies in the location of charged particle absorption signatures associated with the sweeping effects of the Uranian satellites [*Acuna et al.*, 1988], nor can it explain why some H_2 band emissions fall partly outside the Q_3 auroral zone [*Herbert and Sandel*, 1994].

One of the goals of our study is to find out how the octupole of the Uranian magnetic field contributes to the field configuration, and whether it can better explain some of the observations such as the V2 Ultraviolet Spectrometer (UVS) data. In this paper, both the Q_3 model and the Q_3 plus the octupole model (called OCT after *Herbert and Sandel* [1994]) are used for comparison. Although the coefficients for the octupole in the harmonic expansion obtained by *Connerney et al.* [1987] are not unique, the octupole is necessary for better fitting the Uranian magnetic field data. Also, it was found that the octupole changes the shape of the polar cap and alters the plasma flow pattern [*Selesnick*, 1988]. In studying the contributions of high degree multipoles of the magnetic field of Neptune, *Ho et al.* [1997] found that higher degrees (from the fourth to the eighth) obtained by *Connerney et al.* [1991], though not uniquely defined, modify significantly the magnetic field structure in the vicinity of the planet and the field line footprints on the planet surface.

They also found that inclusion of all eight terms in the expansion better explains the UVS data. In view of these, one should keep in mind that results obtained from the OCT model can only be treated in a general sense because of the nonuniqueness of the octupole; on the other hand, the OCT model is not superfluous as the octupole does exist and is nonnegligible.

In studying the relation of plasma dynamics to the magnetic field configuration, the L shell is often used. Because of the high non-dipolar field, it is difficult to obtain a simple definition of L and various definitions were adopted [e.g., *Acuna et al.*, 1988; *Herbert and Sander*, 1994]. In this paper, we use the Euler potentials, or α and β coordinates, to define the coordinates of the magnetic field. The Euler potentials are closely related to the geometrical structure of the magnetic field, and have been proven a convenient tool to describe a highly non-dipolar field like that of Neptune [*Huang and Yu*, 1995; *Ho et al.*, 1997]. In this paper, the same technique of constructing the Euler potentials as used by *Ho et al.* [1997] is used, and a brief discussion of it is given in the following section. In the third section, we shall examine the relationship of the V2/UVS data and the magnetic field configuration of Uranus using both the Q_3 and OCT models.

In order to shed some light onto the question of how the peculiar magnetic field of Uranus affects the plasma dynamics in its inner-magnetosphere, we calculate in the last section the drift paths and drift velocities of charged particles. For simplicity, we limit ourselves to particles that have zero adiabatic invariant ($J = 0$). The drift paths of these particles are then examined in terms of their energies and Uranus' magnetic field configuration, and their association with the UV emissions are sought.

2. The Magnetic Field of Uranus

2.1 Euler potentials and their construction

On the basis of the relationship between the Euler potentials and the geometry of the magnetic field [*Huang and Yu*, 1995], *Ho et al.* [1997] calculated the Euler potentials for the Neptunian magnetic field and examined the details of the field structure. In many respects, the Uranian magnetic field is similar in complexity to that of Neptune. In the OTD representation, Uranus has an angle of dipole inclination (58.6°) which exceeds that of Neptune (46.9°), and the dipole center is off-centered (by 0.33 R_U compared to 0.55 R_N for Neptune). The large dipole tilt and large ratio in the polar magnetic field strengths are two principal sources of the complexity.

The complexity of Uranus' magnetic field is also revealed in the large non-dipolar ($n >$ 1) Schmidt coefficients g_n^m and h_n^m of degree n and order m in the spherical harmonic expansion of the magnetic scalar potential V given by [e.g. *Chapman and Bartels*, 1940]

$$V(r,\theta,\phi) = \sum_{n=1}^{\infty} \sum_{m=0}^{n} \left(\frac{1}{r}\right)^{n+1} \left(g_n^m \cos(m\phi) + h_n^m \sin(m\phi)\right) P_n^m(\cos\theta) \qquad (1)$$

where $P_n^m(\cos\theta)$ are the Schmidt-normalized associated Legendre functions. The first three degrees of the Schmidt coefficients were determined by *Connerney et al.* [1987] which constitute the Q_3 model when only the dipole (n = 1) and quadrupole (n = 2) terms are used. The Schmidt coefficients for the third term are largely unresolved and the inclusion of

them in (1) constitutes the OCT model. Both the Q_3 and the OCT models are used in this paper.

Equation (1) is commonly written in the rotation coordinate system, in which the z-axis and the rotation axis are aligned. Since the values of the α and β coordinates we use are calculated from a knowledge of their values for a dipole field at the initial points, it is necessary to transform (1) into a frame in which the magnetic field can be represented by a dipole field at large enough distance from the planet (> several tens of planetary radii). In this dipole frame, g_1^0 is the only nonzero dipole term and the dipole axis defines the z-axis of the coordinate system. The transformation of the Schmidt coefficients into the dipole frame can be done by integrating (1) using the orthogonal property of $P_n^m(\cos\theta)$ and the geometrical relationship between the two frames (*see Ho et al.,* [1997] for details). The Schmidt coefficients in the dipole frame (unprimed) are given in Table 1 together with those obtained by *Connerney et al.* [1987] in the rotation frame (primed).

To construct the α, β coordinates (same method used in both the Q_3 and OCT model), we start from the zero magnetic scalar potential surface ($V = 0$). The initial values of α and β are defined at $r = 64\ R_U$ and $\theta = 90°$ (in the dipole frame) where the radial distance is large enough that the field is a good approximation to a dipole, and α and β are given by

$$\alpha = g_1^0 \frac{\sin^2\theta}{r} \tag{2}$$

$$\beta = \phi \tag{3}$$

where g_1^0 (22837 nTR_U^3) is the dipole moment in the dipole frame such that g_1^1 and h_1^1 are equal to zero. The reference line of constant α at $r = 64\ R_U$, namely α_o, is calculated from (2) to be 357 nTR_U^3, this line of constant α is divided into 2π shared uniformly to give the values of the Euler potential β. The Euler potential β is numerically equal to the azimuthal angle ϕ in the dipole frame measured from the plane that contains both the rotation axis and the dipole axis. The lines of constant β are constructed along the principal normal of the field line towards the planet [*Huang and Yu*, 1995], thus the values of β defined as the values of ϕ at $r = 64\ R_U$ are mapped over the $V = 0$ surface.

To determine the values of α inside the radial distance $r = 64\ R_U$ on the $V = 0$ surface, we choose an adjacent line $\beta + \Delta\beta$ for each line of constant β, which is also constructed in the same way along the principal normal direction, and use the relation

$$|\mathbf{B}|\Delta S = \Delta\alpha\Delta\beta \tag{4}$$

where $|\mathbf{B}|$ is the magnitude of the magnetic field, ΔS is an element of area, and $\Delta\alpha$ and $\Delta\beta$ are ranges of α and β that bound this element of area. The new value of α on this line of constant β can then be calculated by

$$\alpha = \alpha_o + \frac{1}{\Delta\beta}\int |\mathbf{B}|dS \tag{5}$$

After the Euler potentials on the zero magnetic scalar potential surface are calculated, using $\mathbf{B} \times \mathbf{dl} = 0$ (where $\mathbf{dl}$ is the increment along the field line) and using the constancy of α and

β on each field line, the values of Euler potentials can be mapped from this surface to space and onto Uranus' surface.

2.2 The magnetic field configuration of Uranus

Figure 1a shows the contours of α and β on the zero magnetic scalar potential surface ($V = 0$) for the Q_3 model, a similar plot for the OCT model is shown in Figure 1b. These figures are shown in the rotation frame in which the z-axis is identical to the rotation axis which points approximately to the sun during V2's visit. The xz plane defines 0°W (west longitude) in the Uranus Longitude System (ULS) adopted by *Ness et al.* [1986]. The lines of constant β are shown as the 72 radial lines in Figure 1; their values are from zero increasing uniformly by $\pi/36$. The values of the lines of constant α increase from α_o at $r =$ 64 R_U according to $\alpha = \alpha_o exp(n/5)$ where n is an integer which increases linearly from 0. The four lines of constant α shown in Figure 1 are for $n = 15$ to 19, and $n = 19$ represents the last complete line of constant α, i.e. $r > 1$ everywhere.

Both surfaces in Figure 1 are warped and that of the OCT model is more severe in certain regions. Warped magnetic equator (minimum B surface) of Uranus as well as Neptune has also been shown by *Acuna et al.* [1988; 1993]. In the case of Neptune, *Ho et al.* [1997] shows that both the zero magnetic scalar potential surface and the magnetic equator lie very close to each other except for certain regions very near the planetary surface. These two surfaces also lie in proximity in the case of Uranus. The region in which the two surfaces show significant differences, which occurs only in the OCT model, is indicated by χ in Figure 1b, located roughly from 220°W to 300°W. The $V = 0$ surface in this region opens up a gap as can be clearly seen from the branching of the two adjacent

lines of constant β marked by the heavy lines in the figure. This region represents the most significant difference between the Q3 and OCT models. The shape of the magnetic field lines threading this region, as well as the footpoints of these field lines, are quite different for these models, as we shall see in the following.

Figures 2a and 2b show a set of field lines through the α, β crosspoints on the $V = 0$ surfaces of figures 1a and 1b for the line of constant $\alpha = \alpha_o exp(17/5)$, i.e. the field lines lie on the surface of constant α of this value. Comparing the north (N) and south (S) magnetic poles, a stronger field strength at the S pole is clearly shown. In the OTD model, the stronger S pole is represented by the offset of the dipole center towards the south. For Uranus, the offset is as much as 0.33 R_U from the dipole center. There are little differences in the S pole of the Q_3 (Figure 2a) and OCT (Figure 2b) model. The N poles, on the other hand, are distorted and more open in the OCT model. The distorted area comes from the field lines that thread the region marked with an χ in figure 1b. These field lines spread out as they approach the N pole, resulting in quite different field line footpoints on Uranus surface from the Q_3 models, as we shall show in the next section. Compared to the results of the Q_3 mode, the field lines of the OCT model are more distorted and the resultant N pole is wider open. A different OCT N pole was also noted by Selesnick [1988].

Figures 3a and 3b show another set of field lines through the α, β crosspoints on the $V = 0$ surfaces of figure 1a and 1b for the line of constant $\beta = 3\pi/4$, i.e. the field lines lie on the surface of constant β of this value. These field lines are chosen to be those which go through the vicinity of the region marked by χ in Figure 1b, they are field lines that go through one of the thick lines (lines of constant β) shown. The effects of the inclusion of

the octupole are obvious, the field lines are highly distorted near the planetary surface. The severely warped $V = 0$ surface and the distorted field lines due to the higher magnetic moments affect the position of the magnetic equator, footpoints on the planetary surface, and the drift paths of particles. Particle precipitation along these distorted field lines change the location of possible emission from the ionosphere, which will be discussed in the next session.

3. UV emissions and their association with the magnetic field

During the V2 encounter with Uranus, the Ultraviolet Spectrometer (UVS) onboard observed auroral emission of type H_2 and H Lyman α from a well-confined region localized near the south magnetic pole [*Broadfoot et al.*, 1986]. Later on, *Herbert and Sandel* [1994] analyzed the emission in details and produced an emission intensity map showing aurora at both magnetic poles. The N aurora is stronger than the S aurora consistent with a weak N field and strong S field predicted by the OTD and the Q_3 model. The aurorae at both poles are localized in magnetic longitude and do not show the ringlike aurora around the poles as does the Earth's aurora. The localization of aurora on the central magnetotail magnetic longitude at both poles led *Herbert and Sandel* [1994] to suggest that the magnetotail plasma sheet is the source of the precipitating particles. In this section, we look at the UV emission from the Uranian surface again and reexamine its characteristics and origins in association with the magnetic field structure we presented in the previous section. Again, both the Q_3 and the OCT model will be used.

Plates 1a and 1b show the H_2 band emission map in which the intensity color contours are plotted versus ULS longitude and latitude. Overlaid on the figures are the α, β contours on the planetary surface for the Q_3 model (Plate 1a) and OCT model (Plate 1b). The intensity map is obtained from the same data set that produced the intensity line contours in Figure 2 of *Herbert and Sandel* [1994]. The difference is that the intensity in *Herbert and Sandel* [1994] is set to zero if the estimated brightness is less than the estimated error, while we lower the minimum cutoff for the estimated brightness for the intensity. We shall see that some regions of low intensity which were not shown in *Herbert and Sandel* [1994] provide hints on how the emissions are associated with the magnetic field configuration.

The line contours in Plate 1 are footpoints of the lines of constant α and β on the planetary surface obtained by mapping along the field lines from the α and β contours on the $V = 0$ surface (Figure 1) . Two readily seen differences between the set of contours obtained from the Q_3 and OCT model are the shape and position of the N pole and the larger "open area" in the northern hemisphere at longitudes about 225°W and westward in the OCT model. The difference in the shape of the N pole can also be seen in Figure 2. The larger open area of the OCT model is a result of the field line divergence around the region marked by χ in Figure 1b (see also Figure 2b). In studying the magnetic field of Neptune, *Ho et al.* [1997] found regions like that marked by χ in Figure 1b containing a local magnetic field system with its own closed particle drift paths. Such a region is a consequence of the non-dipolar moment of the magnetic field, and though small on the $V =$

0 surface, may open up a large area on the planetary surface on which only field line footprints of this localized magnetic system can impinge.

The emission "hot spot" reported by *Broadfoot et al.* [1986] and *Herbert and Sandel* [1994] are shown in Plate 1 as red, yellow and green contours near the N and S magnetic pole. If all the auroral emissions near the poles are considered (i.e. including the blue and purple contours), they appear as two partial rings centered on the N and S magnetic poles. The portion of the ring that shows no emission is in the geographical northern section of each aurora, roughly coinciding with the "gaps" in the α contours. If the emissions and the contours of α and β do indeed have a certain relationship, one may interpret the Uranian aurora as a ring shape round the poles like those of the Earth, but the rings are not complete due to the unique magnetic field line structure. The OCT model explains the UVS data better because of the larger open area that it yields, for instance, the area around 270°W towards the south of the geographical equator has no contours of α and β and therefore no emission. While the S pole of both models do not show much difference, the OCT provides a better magnetic N pole around which the emissions are centered.

4. Particle drifts in Uranus' inner-magnetosphere

The study of particle's drift motion is important for understanding the magnetic configuration, and helpful to the interpretation of the observed particle absorption signatures and radiation emission spectra such as the UV emissions. In this section, we calculate the particle drift and the drift velocity within about 5 R_U of Uranus. Because of the complicated nature of the drift, we limit the calculation to charged particles of zero second

invariant ($J = \int v_{\parallel} ds = 0$), i.e. particles with no bounce motion. For a $J = 0$ particle of mass m, the total energy is

$$K = \mu B - \frac{mGM}{r} - \frac{1}{2} m\Omega^2 r_{\perp}^2 \tag{6}$$

where G is the universal gravitational constant, M and Ω are the mass and rotational frequency of the planet, r and $r_{\perp}$ are the distances from the planet's center and its rotation axis, and μ is the magnetic moment of the particle.

For a non $J = 0$ particle, there are in general two mirror points on a field line between which the particle bounces (except a field line that has its magnetic field strength changing monotonically from one end to the other or a field line that has multiple mirror points). On one field line, a particle that has the same total energy but a larger pitch angle (greater μ) has its mirror points closer together, so a particle that has no bounce motion, i.e. with one mirror point, stays at the position where the particle has a maximum value of μ and the component of total force applied on the particle is equal to zero. Therefore in order to trace out the drift paths of the $J = 0$ particles, we first determine the surface of maximum μ for a particle with a given total energy, after that, we compute the contours of μ on the maximum μ surface, which give the particle drift paths.

The sum of the gradient drift, and drifts due to gravity and centrifugal force, is given by

$$\mathbf{v}_d = \frac{\mu}{q} \frac{\mathbf{B} \times \nabla \mathbf{B}}{B^2} + \frac{1}{qB^2} \left[-\frac{\mathrm{mMG}}{r^3} \mathbf{r} - \mathrm{m}\boldsymbol{\Omega} \times (\boldsymbol{\Omega} \times \mathbf{r}) \right] \times \mathbf{B} \tag{7}$$

Note $\mathbf{v}_d$ is not the actual drift velocity **u** which lies on the maximum μ surface, rather, it is the component of **u** perpendicular to the field line. The actual drift velocity **u** is the sum of $\mathbf{v}_d$ and a component $v_{||}$ parallel to the field line. Here the particle's second invariant $J = 0$ still holds although there exists a field-aligned drift velocity component $v_{||}$, because $v_{||}$ has a higher order of magnitude than $\mathbf{v}_d$. The magnitude of the actual drift velocity **u** can be calculated from $\mathbf{v}_d$ by

$$u = \frac{v_d}{\cos \xi} \tag{8}$$

where ξ is the angle between **u** and $\mathbf{v}_d$.

The drift paths and velocities depend on both the particle's kinetic energy, μB, and the gravitational and centrifugal energies. For energetic particles, the total potential energy is small compared to the kinetic energy, the drift velocity is largely the result of gradient drift (first term of Equation 7). Setting the last two terms of (6) to zero, we can see that the maximum μ surface is also the minimum B. Therefore energetic particles of $J = 0$ drift on the magnetic equatorial plane, which is approximately the $V = 0$ surface shown in Figure 1. In addition, the drift paths are approximately the lines of constant magnetic field strength since μ is a constant and the kinetic energy μB is near a constant for energetic particles. Plate 2 shows the drift paths of particles of total energy 10 eV for the OCT model. Because Uranus has a North to South magnetic flux, the ions drift in the West-East direction opposite to that of the Earth, while the electrons drift in the East-West direction. Following the above discussions, the drift paths are approximately the minimum B contours, thus they are roughly concentric except very near the planetary surface where the contribution of the non-dipolar terms become more significant. Plate 2 thus represents the drift paths of all $J =$

0 particles of energies of a few eV and above, except the magnitudes of the drift velocity are greater for greater energy.

For low energy ions that have kinetic energy comparable to the sum of gravitational and centrifugal energies, the magnitude of the drift velocity depends not only on the magnetic gradient but also strongly on gravitational and centrifugal forces. The maximum μ surface for total energy of – 0.8 eV is shown in Plate 3, also for the OCT model. This surface deviates from the minimum B surface (not shown), particularly for small r. The distorted drift surface and the great variations in magnetic field intensity on this surface are responsible for the non-symmetrical drift pattern shown for low energy ions. Because the drift due to gravity is in opposite direction to those produced by magnetic gradient and centrifugal force, the drift may reverse direction in some region. There may even be local trapped particles circulating. Plate 3 shows that a large number of particles do not complete a 360° drift.

Plates 1a and 1b also show where the low energy particle drift surface (maximum μ surface) intercepts the planetary surface (green filled circles), also shown in the plates are similar interception lines for the high energy particle drift surface (minimum B surface, blue filled circles) and the $V = 0$ surface (red filled circles). It is clear that some of the UV emission "islands" are along those interception lines, they are marked by A, B and C in Plate 1b. These locations coincide with those similarly marked locations in Plate 3 where the particle drifts converge onto the planetary surface. It is therefore quite conceivable that some of the UV emissions observed are due to precipitation of $J = 0$ particles or particles that have large pitch angles into the atmosphere along the magnetic equatorial regions.

Emissions from regions such as A and B may also be due to the converging of field lines into these regions. The converging of the field lines to two localized regions can be seen clearly from the "broken" donut-shaped surface of constant α in Figure 2b, which collapses along the two edges onto the planetary surface. UV emission associated with the concentration of field lines has also been reported for Neptune [*Ho et al.*, 1997]. The region marked C is a region of special interest. This is where the surfaces of low energy particle drift (green), high energy particle drift (blue), and $V = 0$ (red) show the greatest differences. In this region, field lines do not have a maximum μ for low energies and some field lines are monotonic.

The magnitudes of the charged particle drift velocities are represented by the color contours in Plates 2 and 3 for total energies of 10 *eV* and –0.8 *eV*, respectively. The magnitude of drift velocity of the 10 *eV* particles vary from less than 0.1 *m/s* near Uranus' surface to about 1.5 *m/s* at $r = 5\ R_U$, corresponding to values of μ from $5 \times 10^{-14}\ Am^2$ to $5 \times 10^{-12}\ Am^2$. The magnitude of velocity does not change much along each constant line of μ, in other words, it is roughly symmetric about the dipole axis. The magnitude of drift velocity of particles with a total energy of –0.8 *eV* (comparable kinetic and potential energies) vary from 0.001 *m/s* near Uranus' surface to 0.1 *m/s* at $r = 5\ R_U$, corresponding to values of μ from $5 \times 10^{-15}\ Am^2$ to $2 \times 10^{-13}\ Am^2$. The drift velocities are particularly low in two regions roughly along the x-axis, i.e. along the plane that contains the rotation and dipole axes. Along this axis a point on the $V = 0$ surface has a cylindrical distance that is the shortest compared to the radial distance, the contribution to the drift from the centrifugal force is therefore the smallest; and because the drifts due to gravity and

centrifugal force are opposite, the drift direction changes and circulating particles may exist in these two regions.

4. Summary and Discussion

Using *Connerney et al.*'s [1987] Q_3 and OCT model for Uranus' magnetic field, we constructed the magnetic field lines within a distance of about 5 R_U using the Euler Potentials as a magnetic field representation. We found the octupole significantly modifies the field line structure within 3 R_U around 250°W. The footpoints of the field lines through this region leave out a large open area on the planetary surface spanning more than 180° westward from 220°W, and extending from the geographical north pole to the equator. Compared with the results of the Q_3 model, the OCT model seems to provide a better Uranian magnetic field configuration to explain some of the V2/UVS data. The large open area in the northern hemisphere may explain why Uranus' aurorae do not encircle the N and S poles like that of Earth's, and the N magnetic pole of the OCT model provides a better position for the N aurora to center upon.

Up to now, the octupole of the Uranian magnetic field have been largely ignored in various studies of Uranus because the octupole terms in the spherical harmonic expansion are not well-resolved. The octupole was used in *Selesnick* [1988] as a comparison with the Q_3 model's results in studying magnetospheric convection, and the conclusion was made that the octupole alters the shape of Uranus' polar cap as well as the convection pattern. *Herbert and Sandel* [1994] also used both the Q_3 and OCT model in their analysis of V2's

UVS data, although without strong evidence, the OCT model does seem better to organize the UVS data, especially the distribution of the aurorae along the latitude. Our results lend a much stronger support to the OCT model. Not only the strong UV emission can better be explained in terms of the α and β coordinates based on the OCT, the weak emission lies in a belt coincides remarkably well with the OCT magnetic equator.

In a similar study of Neptune's magnetic field, *Ho et al.* [1997] also concluded that the higher degrees (fourth to eighth) of the harmonic expansion of the field could better explain some of the UVS data. Since the closest approach of V2 to Uranus is only 4.2 R_U compared to 1.2 R_N to Neptune, it is conceivable that the magnetic field of Uranus also contain significant higher moments which would further modify the magnetic field structure near the planet and provides a better framework for analyzing the observed data. It is quite remarkable that the analysis of the magnetometer data along a limited path of the satellite trajectory yields a map of magnetic coordinates on the planetary surface that so successfully explain some of the features of the emission data. The unresolved coefficients in these models may not be well resolved and the values may not be unique; however they do seems represent a fairly accurate picture of the field. In view of this, we feel the OCT magnetic field model for Uranus, like the I8E1 model for Neptune, deserves more merit than it has already received.

Acknowledgments. We would like to thank F. Herbert for providing us the analysis of the Voyager UVS data for making our Plates 1a and 1b. This work is supported by NASA Grant NAG 5-2317 and JPL contractor 961073.

References

Acuna, M. H., J. E. P. Connerney, and N. F. Ness, Implications of the GSFC Q3 model for trapped particle motion, *J. Geophys. Res.*, 93, 5,505, 1988.

Acuna, M. H., J. E. P. Connerney, and N. F. Ness, Neptune's magnetic field: Calculation of field geometric invariants derived from the I8E1 GSFC/BRI model, *J. Geophys. Res.*, 98, 11,275, 1993.

Broadfoot, A. L., F. Herbert, J. B. Holberg, D. M. Hunten, S. Kumar, B. R. Sandel, D. E. Shemansky, G. R. Smith, R. V. Yelle, D. F. Strobel, H. W. Moos, T. M. Donahue, S. K. Atreya, J. L. Bertaux, J. E. Blamont, J. C. Mcconnell, A. J. Dessler, S. Linick, R. Springer, Ultraviolet spectrometer observations of Uranus, *Science,* 233, 74, 1986.

Chapman, S., and J. Bartels, *Geomagnetism,* pp. 639-668, Oxford university Press, New York, 1940.

Connerney, J. E. P., M. H. Acuna, and N. F. Ness, The magnetic field of Uranus, *J. Geophys. Res.*, 92, 15,329, 1987.

Connerney, J. E. P., M. H. Acuna, and N. F. Ness, The magnetic field of Neptune, *J. Geophys. Res.*, 96, 19,023, 1991.

Herbert F., and B. R. Sandel, The Uranian aurora and its relationship to the magnetosphere, *J. Geophys. Res.*, 99, 4143, 1994.

Ho, C. W., T. S. Huang, and S. Gao, Contributions of the high degree multipoles of Neptune's magnetic field: an Euler potentials approach, *J. Geophys. Res.*, *102*, 24,393, 1997.

Huang, T. S. and X. Yu, Magnetic field geometry and the α, β coordinate system, F497, 76, Eos, *Transactions,* AGU, 1995.

Mauk, B. H., S. M. Krimigis, E. P. Keath, A. F. Cheng, T. P. Armstrong, L. J. Lanzerotti, G. Gloeckler, and D. C. Hamilton, The hot plasma and radiation environment of Uranian magnetosphere, *J. Geophys. Res.,* 92, 15,283, 1987.

Ness, N. F., M. H. Acuna, K. W. Behannon, L. F. Burlaga, J. E. P. Connerney, R. P. Lepping and F. M. Neubauer, Magnetic fields at Uranus, *Science,* 233, 85, 1986.

Selesnick, R. S., Magnetic convection in the nondipolar magnetic field of Uranus, *J. Geophys. Res.,* 93, 9607, 1988.

Selesnick, R. S., and J. D. Richardson, Plasmasphere formation in arbitrarily oriented magnetospheres, *Geophys. Res. Lett.*, *13*, 624, 1986.

Vasyliunas, V. M., The convection-dominated magnetosphere of Uranus, *Geophys. Res. Lett.*, 13, 621-623, 1986.

Figure Captions

Figure 1a. Contours of α and β on the zero magnetic potential surface for the Q_3 model. The values of α increasing according to $\alpha = \alpha_o \, exp(n/5)$ where α_o is the value of α at $r =$ 64 R_U and $n = 0,1,2...$ The four lines of constant α shown are for $n = 15$ to 19 and the inner most one ($n = 19$) is the last line of constant α for $r > 1$. The lines of constant β have values increasing by $\pi/36$ starting from 0.

Figure 1b. Similar surface as Figure 1a but for the OCT model. The lines of constant β diverge in the region marked by χ and the footpoints of field lines through this region leave large open spaces on the planetary surface.

Figure 2a. Magnetic field lines on the surface of constant $\alpha = \alpha_o \, exp(27/5)$ of the Q_3 model.

Figure 2b. Similar plot as Figure 2a except for the OCT model. The surface shown here has a large open gap where the magnetic fields collapse onto the planetary surface.

Figure 3a. Magnetic fields through the line of constant $\beta = 3\pi/4$ for the Q_3 model. The field lines are near dipole shape.

Figure 3b. Similar plot as Figure 3a except for the OCT model. Field lines near the planet are severely distorted due to the octupole moments.

Plate 1a. UV emissions in color contour plotted against ULS latitude and west longitude (right most longitude is 0°W). Overlaid are α and β contours of the Q_3 model that are mapped along the field lines from the zero scalar potential surface ($V = 0$) shown in Figure 1a. Also shown are the interception of the low energy particle drift surface with the planetary surface (green filled circles), as well as the similar interception lines of the high energy particle drift surface (blue filled circles) and the V = 0 surface (red filled circles). The blue filled circles also mark the magnetic equator (minimum B). The UVS data are similar to *Herbert and Sandel* [1994] except some low emissions which were ignored by *Herbert and Sandel* are shown here.

Plate 1b. Same as Figure 1a except for the OCT model. The UVS data are the same as those in Plate 1a.

Plate 2. Drift velocities (color contours) and drift paths (black lines) of particles of total energy 10 eV using the OCT model.

Plate 3. Similar plot as Plate 3 except for particle of energy –0.8 eV. Regions marked with A, B and C correspond to those similarly marked regions in Plate 1b. Particle drift paths converge to these regions.

Table 1. Normalized Schmidt's spherical harmonic coefficients of the Uranus magnetic field model in the rotation frame (primed) and dipole frame (unprimed) frame. The Q_3 model uses only the first expansion coefficients and the OCT uses all three.

n	m	$g_n^{'m}$	$h_n^{'m}$	g_{nm}	h_{nm}
1	0	11,893	0	22,837	0
1	1	11,579	–15,684	0	0
2	0	–6,030	0	–11,891	0
2	1	–12,587	6,116	8,268	–4,418
2	2	196	4,759	–1,222	4,911
3	0	2,705	0	3,756	0
3	1	1,188	–7,095	–5,511	–2,012
3	2	–4,808	–1,616	4,737	5,081
3	3	–2,412	–2,608	396	698

Table 1

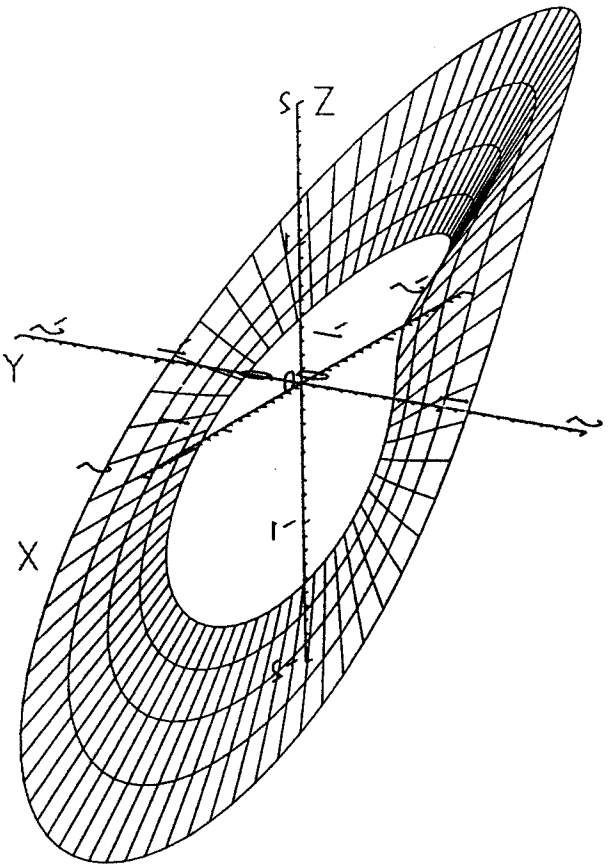

Figure 1a

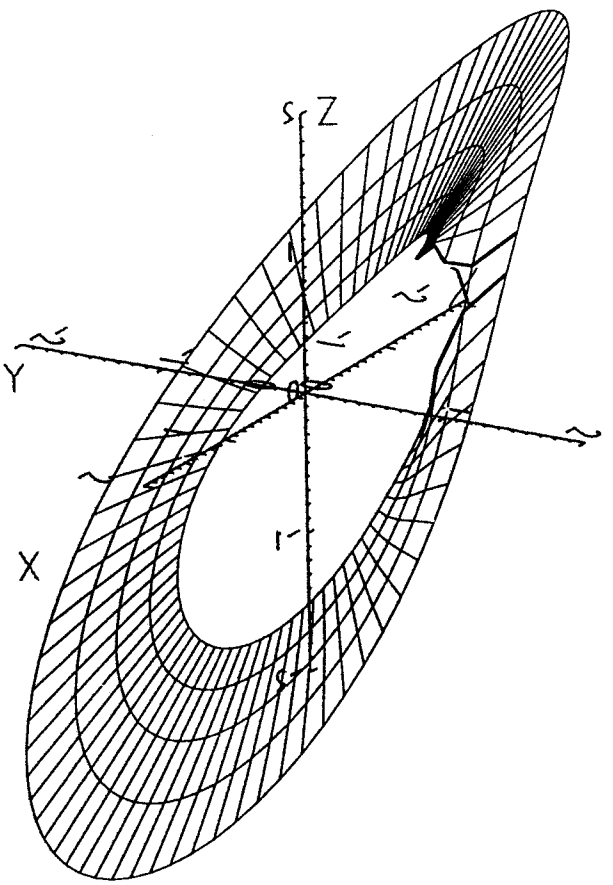

Figure 1b

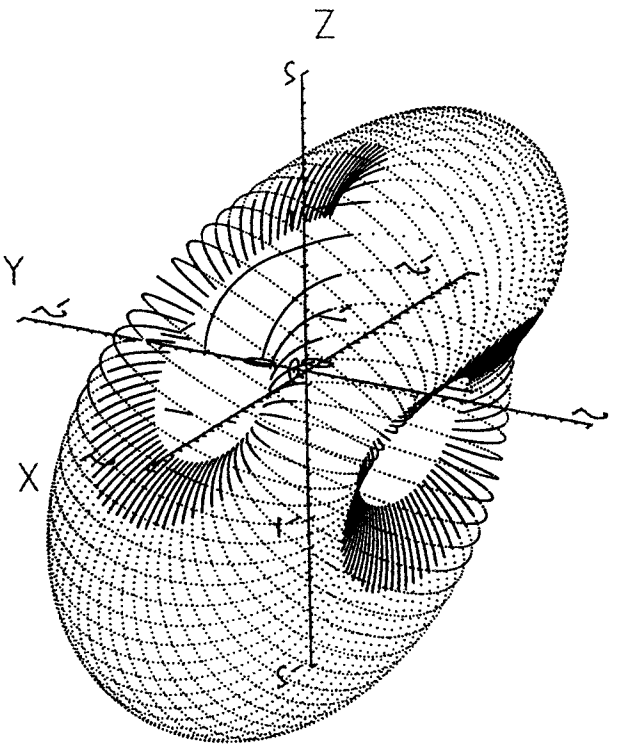

Figure 2a

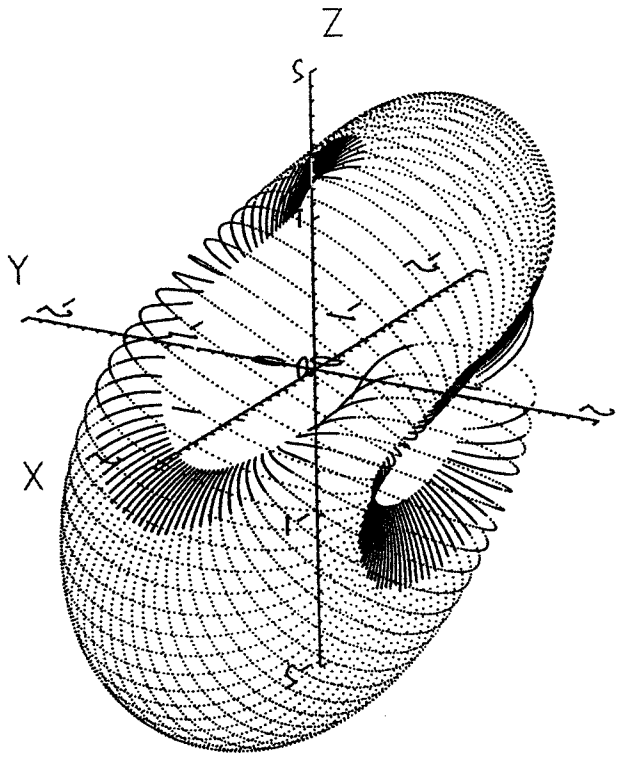

Figure 2b

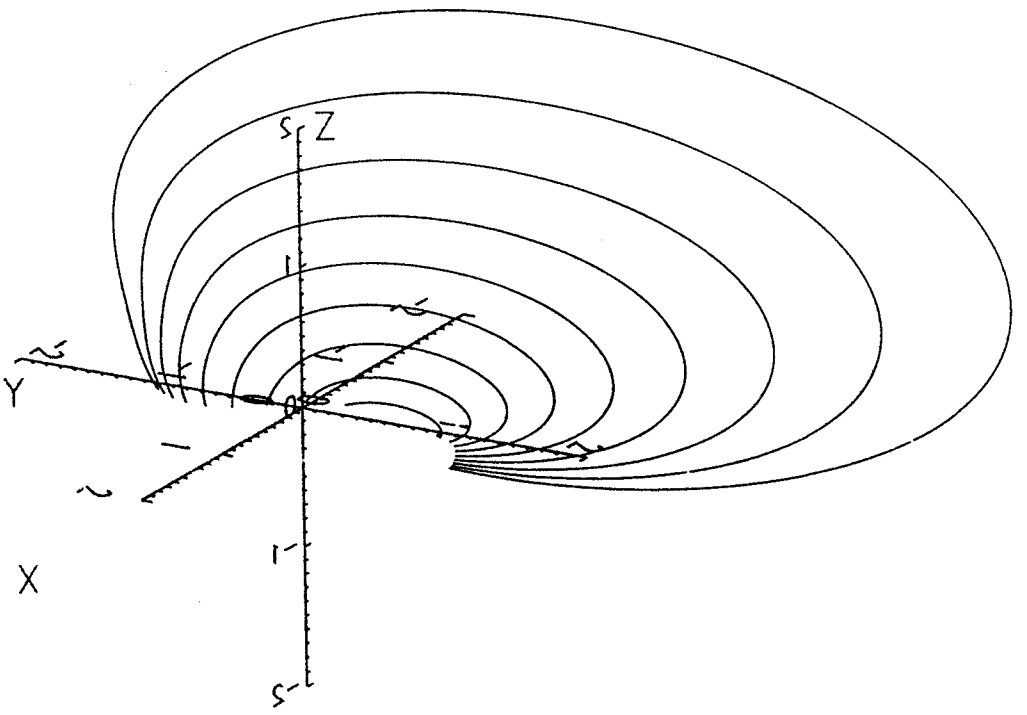

Figure 3a

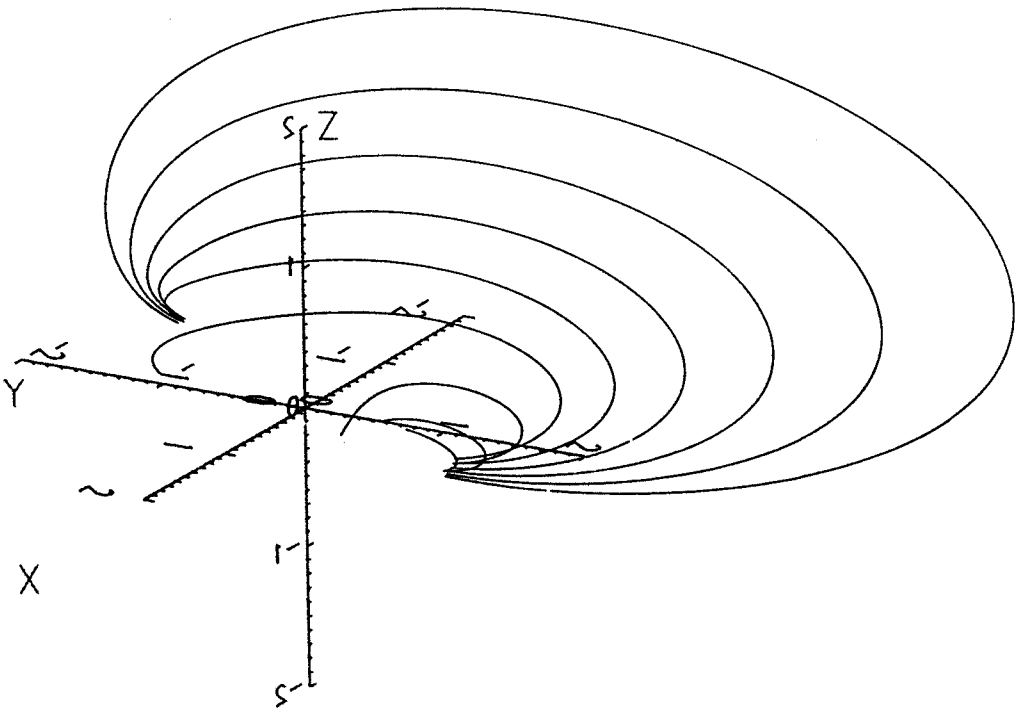

Figure 3b

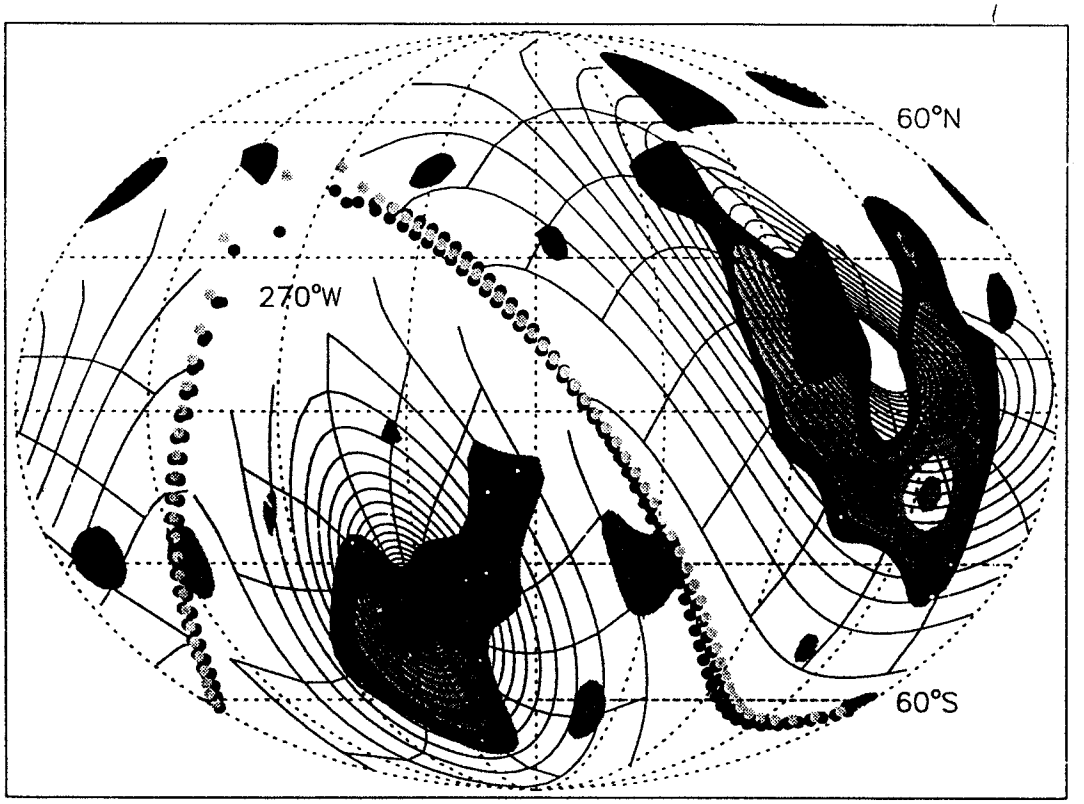

Normalized Intensity

0.0 0.2 0.4 0.6 0.8 1.0

Plate 1a

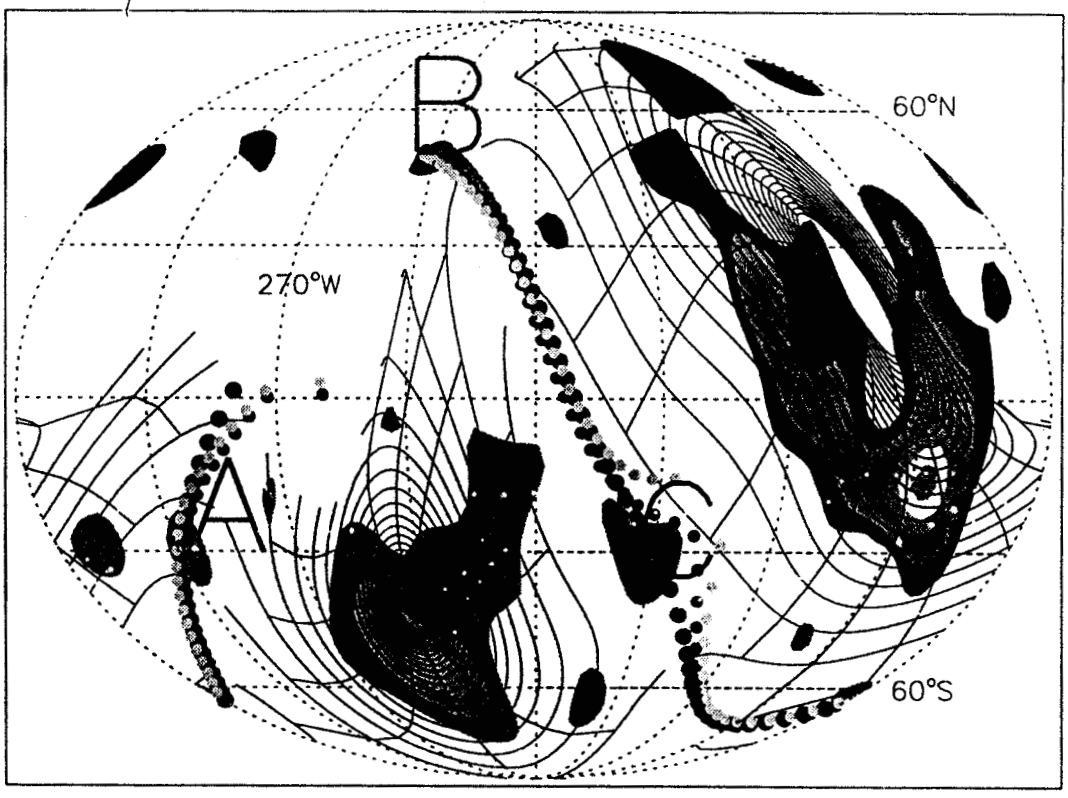

Normalized Intensity

0.0 0.2 0.4 0.6 0.8 1.0

Plate 1b

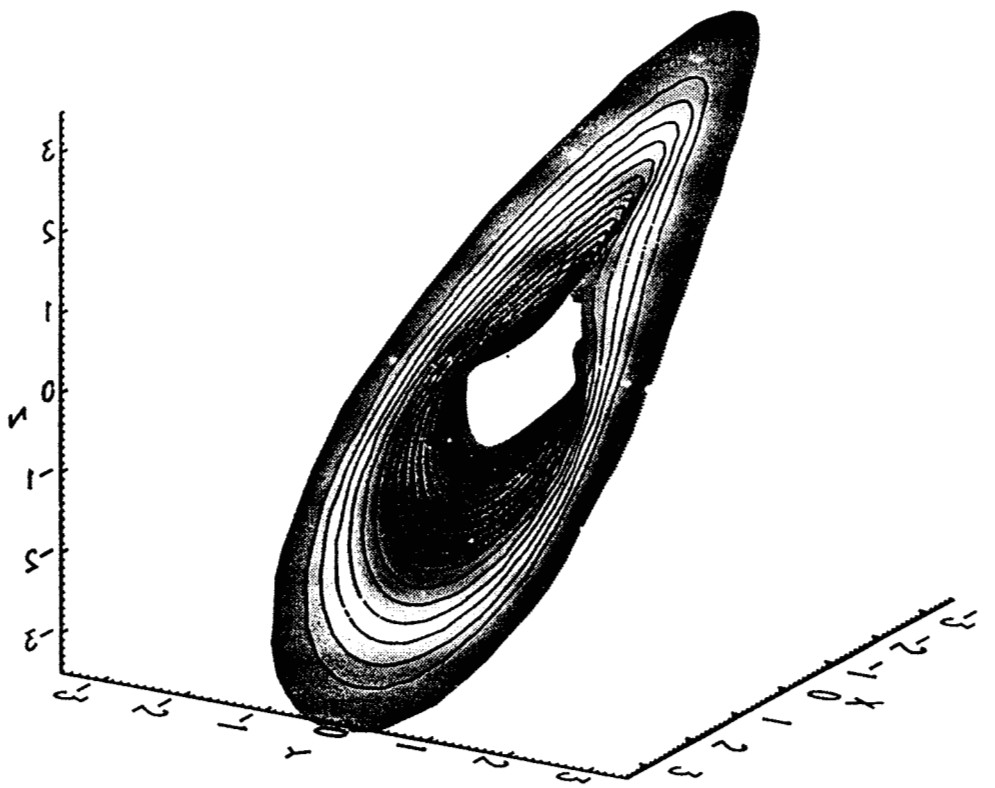

H^+ drift velocity (m/s)

0.2 0.4 0.6 0.8 1.0 1.2 1.4

Plate 2

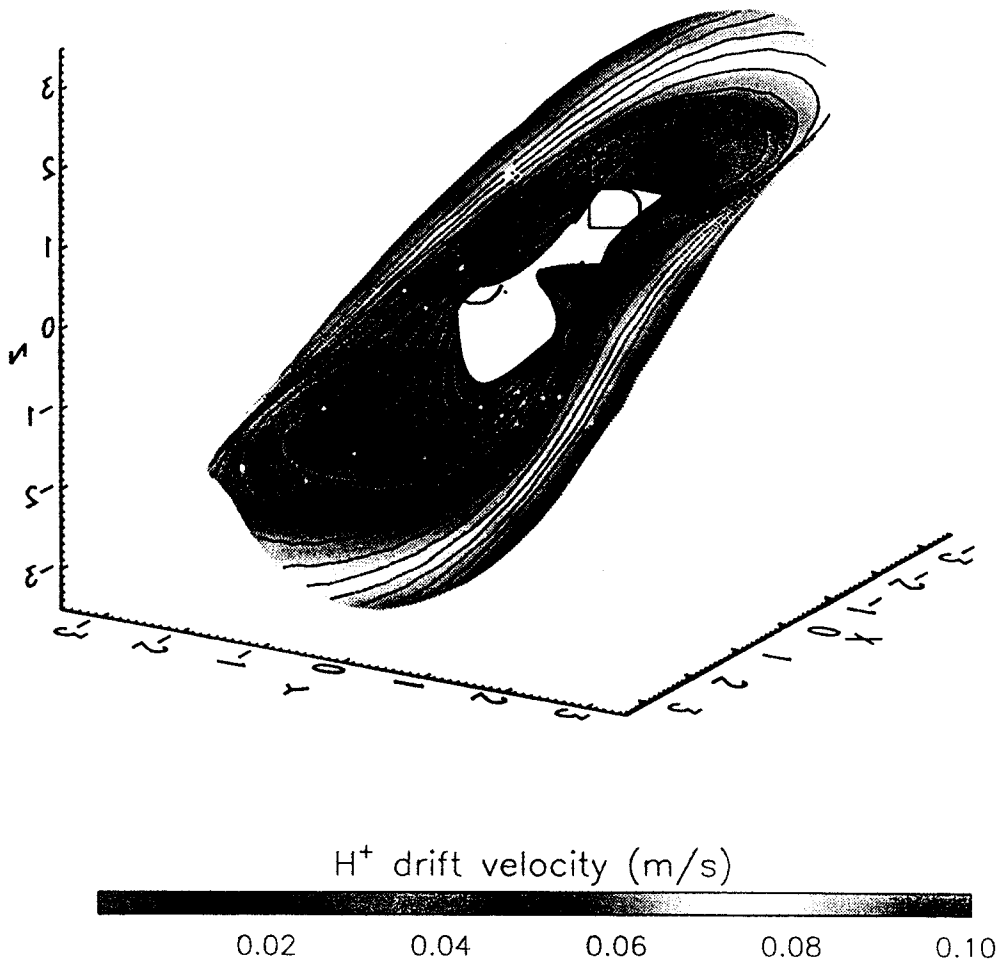

Plate 3